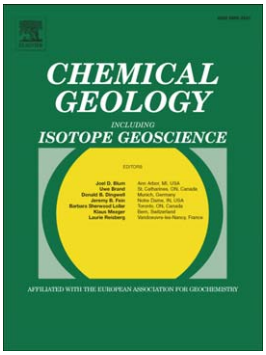

Crystallisation temperatures of the most Mg-rich magmas of the Karoo LIP on the basis of Al-in-olivine thermometry

Jussi S. Heinonen, Eleanor S. Jennings, Teal R. Riley

PII: S0009-2541(15)00303-4
DOI: doi: 10.1016/j.chemgeo.2015.06.015
Reference: CHEMGE 17611

To appear in: *Chemical Geology*

Received date: 13 March 2015
Revised date: 12 June 2015
Accepted date: 16 June 2015

Please cite this article as: Heinonen, Jussi S., Jennings, Eleanor S., Riley, Teal R., Crystallisation temperatures of the most Mg-rich magmas of the Karoo LIP on the basis of Al-in-olivine thermometry, *Chemical Geology* (2015), doi: 10.1016/j.chemgeo.2015.06.015

Crystallisation temperatures of the most Mg-rich magmas of the Karoo LIP on the basis of Al-in-olivine thermometry

Jussi S. Heinonen [a] (PhD, corresponding author, jussi.s.heinonen@helsinki.fi, +35850-3185304)

Eleanor S. Jennings [b] (MSci, esj26@cam.ac.uk, +44-1223-333424)

Teal R. Riley [c] (PhD, trr@bas.ac.uk, +44-1223-221423)

[a] Finnish Museum of Natural History, P.O. Box 44, University of Helsinki, 00014, Helsinki, Finland
[b] Department of Earth Sciences, University of Cambridge, Downing Street, Cambridge CB2 3EQ, United Kingdom
[c] British Antarctic Survey, Madingley Road, High Cross, Cambridge CB3 0ET, United Kingdom

Abstract
Calculating reliable temperatures of Mg-rich magmas is problematic because melt composition and $K_D(Fe\text{-}Mg)^{ol\text{-}liq}$, the key parameters of many traditional thermometers, are difficult to constrain precisely. The recently developed Al-in-olivine thermometer [Coogan, L.A., Saunders, A.D., Wilson, R.N., 2014. Aluminum-in-olivine thermometry of primitive basalts: Evidence of an anomalously hot mantle source for large igneous provinces. Chemical Geology 368, 1–10] circumvents these problems by relying on the temperature-dependent exchange of Al between olivine and spinel crystallising in equilibrium with each other. This thermometer is used to re-evaluate the crystallisation temperatures of the most Mg-rich magma type identified from the Karoo large igneous province (LIP), known as the Vestfjella depleted ferropicrite suite. Previous temperature estimates for the suite were based on olivine-melt equilibria and indicated anomalously high crystallisation temperatures in excess of 1600 °C. We also present crystallisation temperatures for another Antarctic Karoo magma type, Group 3 dykes from Ahlmannryggen, which are derived from a pyroxene-rich mantle source. Our high-precision analysis of Al in olivine-spinel pairs indicate crystallisation temperatures from 1391±42 °C to 1481±35 °C for the Vestfjella depleted ferropicrite suite ($Fo_{88–92}$) and from 1253±64 °C to 1303±40 °C for the Group 3 dykes ($Fo_{79–82}$). Although the maximum temperature estimates for the former are over 100 °C lower than the previously presented estimates, they are still ~200 °C higher than those calculated for mid-ocean ridge basalts using the same method. Although exact mantle potential temperatures are difficult to estimate, the presented results support elevated sub-Gondwanan upper mantle temperatures (generated by a mantle plume or internal mantle heating) during the generation of the Karoo LIP.

Keywords: Karoo; large igneous province; continental flood basalt; picrite; thermometry

1. Introduction

Reasonable constraints on the crystallisation and mantle source temperatures of mantle-derived mafic and ultramafic igneous rocks are crucial for determining the geodynamics of our planet. Yet, this task has long remained one of the major challenges in modern petrological research: e.g., the question of whether large-scale intra-plate volcanic phenomena such as continental flood basalts (CFBs) require the existence of thermal anomalies in the upper mantle has been heavily debated (see Anderson, 2005; Campbell, 2005; Herzberg, 2011). Temperature estimates of mantle-derived magmas have traditionally relied on estimates of (parental) melt and mantle source compositions and/or olivine-liquid equilibration conditions (e.g., Roeder and Emslie, 1970; Ford et al., 1983; Beattie, 1993; Herzberg and O'Hara, 2002; Herzberg et al., 2007; Putirka, 2005; Falloon et al.,

2007; Putirka et al., 2007; Lee et al., 2009; Herzberg and Asimow, 2008, 2015). In the case of CFBs, these are often very difficult to define due to the high degree of differentiation, geochemical overprinting by the assimilation of continental lithosphere, and the lack of knowledge of the geochemistry of CFB primary melts.

Recent advancements in constraining the temperature-dependent behaviour of Al in magmatic olivine and Cr-spinel in equilibrium with each other have provided a new tool to estimate crystallisation temperatures (Al-in-olivine thermometer; Wan et al., 2008; Coogan et al., 2014). Olivine and Cr-spinel are usually the first minerals to crystallise from primitive mantle-derived magmas: during co-crystallisation, the two phases must be in equilibrium with each other. Spandler and O'Neill (2010) demonstrated that Al diffusion within olivine is extremely slow, and so even at low cooling rates, the initial composition of a spinel-olivine pair is preserved. Thus, chemical information is recorded from the earliest stages of magma evolution. Importantly, the application of Al-in-olivine thermometry does not require information on the parental melt compositions and has insignificant pressure dependence (Wan et al., 2008; Coogan et al., 2014). It is thus especially useful in determining the temperatures of CFB magmas.

The ~180 Ma Karoo CFBs (Fig. 1) erupted during the initial stages of the breakup of the Gondwana supercontinent in a developing fracture between the landmasses of modern Africa and Antarctica (e.g., Cox, 1988, 1992; Jourdan et al., 2005, 2007b). The trace element and isotopic compositions of the majority of Karoo CFBs are compatible with melt contribution from the underlying continental lithosphere (e.g., Hawkesworth et al. 1984; Sweeney et al. 1994; Luttinen et al 1998, 2015; Luttinen & Furnes 2000; Riley et al. 2005; Ellam 2006; Jourdan et al. 2007a; Neumann et al., 2011), but rare CFB-related dykes that are not contaminated by the lithosphere and show evidence of both depleted and enriched (recycled) sublithospheric sources have been described from the Antarctic portion of the province (Fig. 1; Luttinen et al., 1998, 2015; Luttinen and Furnes, 2000; Riley et al., 2005; Heinonen and Luttinen, 2008, 2010; Heinonen et al., 2010, 2013, 2014, in press). The so-called "Vestfjella depleted ferropicrite suite" is a magma type that bears evidence of the most Mg-rich melts (MgO > 20 wt. %) known from the Karoo (Heinonen and Luttinen, 2010). The notably high crystallisation and mantle potential temperatures (≥ 1600 °C) calculated on the basis of olivine-liquid equilibria following the method of Putirka et al. (2007) are indicative of mantle plume sources (Heinonen and Luttinen, 2010), but are in glaring contrast with the Sr, Nd, Pb, Os, and He isotopic compositions and trace element characteristics that indicate derivation from upper mantle sources akin to those of the Southwest Indian Ridge mid-ocean ridge basalts (SWIR MORBs) (Heinonen et al., 2010; Heinonen and Kurz, in press).

Most of the Antarctic dyke rocks with sublithospheric geochemical affinities contain fresh olivine with abundant Cr-spinel inclusions (Fig. 2; Heinonen and Luttinen, 2010; Heinonen et al., 2013) and thus provide suitable sample material for the use of the Al-in-olivine thermometer. Given that the previous temperature calculations (Heinonen and Luttinen, 2010) are based on equations of Putirka et al. (2007) that require knowledge on the parental magma compositions and crystallisation conditions (see Falloon et al., 2007) and tend to overestimate temperatures suggested by Al-in-olivine thermometry by around ~100 °C (Coogan et al., 2014), there is a need for reappraisal. Here we present olivine and spinel mineral chemical data for the Vestfjella depleted ferropicrite suite and for another series of Mg-rich primitive dykes (Group 3; Riley et al., 2005) from Ahlmannryggen, western Dronning Maud Land, Antarctica. They represent melting of peridotitic (Heinonen and Luttinen, 2010, Heinonen et al., 2010) and pyroxenitic (recycled oceanic crust mixed with mantle peridotite; Heinonen et al., 2013, 2014) sources in the sublithospheric mantle, respectively. Unlike the majority of the lithosphere-signatured Karoo CFBs, these intrusive rocks provide the best material available for estimating the thermal conditions beneath the thick Gondwanan lithosphere during Karoo magmatism.

2. Geological setting and sample suites

The Jurassic (~180–190 Ma; Duncan et al., 1997; Zhang et al., 2003; Riley et al., 2005, 2009; Luttinen et al., 2015) Karoo CFBs and related intrusive rocks of Antarctica are found up to few hundred kilometres off the coast of western Dronning Maud Land (Fig. 1). The CFBs, exposed at Vestfjella, Heimefrontfjella, and Kirwanveggen, represent the youngest major stratigraphic unit in the area and are underlain by Palaeozoic sedimentary rocks (e.g., Juckes, 1972) and/or a Precambrian basement complex consisting of a variety of Archaean to Proterozoic rocks (e.g., Wolmarans and Kent 1982, Groenewald et al., 1995; Moyes et al., 1995; Jacobs et al., 1998; Marschall et al., 2010). Abundant CFB-related intrusive rocks are found in the same areas, but they also crosscut the basement complex at Ahlmannryggen, Borgmassivet, H.U. Sverdrupfjella, and Mannefallknausane (Fig. 1). The lavas and intrusive rocks can be geochemically divided into several groups, most of which show strong evidence of melt contribution from continental crust and/or lithospheric mantle (Furnes et al., 1987; Harris et al., 1990, 1991; Luttinen et al., 1998, 2010; 2015; Luttinen and Furnes, 2000; Riley et al., 2005). Some of the magma types show geochemical similarities with the larger Karoo CFB formations found on the African side of the Jurassic rift system (e.g., Luttinen and Furnes, 2000; Riley et al., 2005).

Four intrusive magma types from western Dronning Maud Land show evidence of limited lithospheric interaction and derivation of the parental magmas from sublithospheric sources: 1) The Vestfjella depleted ferropicrite suite, 2) Vestfjella Low-Nb dykes, 3) The Vestfjella enriched ferropicrite suite, and 4) Ahlmannryggen Group 3 dykes (Riley et al., 2005; Heinonen and Luttinen, 2008; Heinonen et al., 2010; Luttinen et al., 2015). The first two originated from a common depleted (upper mantle) source (Heinonen et al., 2010; Luttinen et al., 2015) and the latter two derive from distinct pyroxene-rich (recycled) mantle sources (Heinonen et al., 2010, 2013, 2014). In this study, we will concentrate on the depleted ferropicrite suite and Group 3 dykes. Analysis of the Low-Nb dykes is hampered by limited volume of sample-material and alteration of olivine, and analyses of the enriched ferropicrite suite showed spinel compositions that are very Fe^{3+}-rich ($Fe^{3+}/Fe^{T} > 0.40$) and notably outside the calibration range for the Al-in-olivine thermometer ($Fe^{3+}/Fe^{T} \leq 0.35$; Coogan et al., 2014).

The Vestfjella depleted ferropicrite suite is composed of dykes that show a wide range of major element compositions from meimechites to basalts (MgO = 5–28 wt. %) and are composed of variable amounts of olivine, clinopyroxene and plagioclase phenocrysts within a groundmass of basaltic composition (Heinonen and Luttinen, 2008, 2010). Crystalline melt inclusions in olivine contain igneous amphibole that indicates parental melt H_2O contents of 1–2 wt. % (Heinonen and Luttinen, 2010). The most Mg-rich samples have been collected from boulders within glacial drift deposits at Basen nunatak (Fig. 1). The boulders exhibit chilled margin contacts of the high-Mg magmas adjacent to sandstones, and have thus likely been transported and deposited at Basen nunatak from the surrounding valleys (Lindström, 2005). Some of the boulders represent cumulate samples, but others contain very Mg-rich olivine phenocrysts (up to Fo_{92}) in or close to equilibrium with the whole-rock composition (Heinonen and Luttinen, 2010). For the estimation of maximum olivine-spinel equilibrium temperatures, we selected meimechitic boulder sample AL/B1b-03 (MgO = 19 wt. %) that is characterised by abundant forsteritic olivine (with euhedral/subhedral spinel inclusions; Fig. 2a) and is likely to closely correspond to a melt composition (Heinonen and Luttinen, 2010).

The Group 3 dykes (MgO = 8–22 wt. %) crosscut the Precambrian basement rocks of western Dronning Maud Land at Ahlmannryggen (Fig. 1; Riley et al., 2005). In addition to fresh olivine and clinopyroxene phenocrysts, many of the Group 3 dykes also contain orthopyroxene phenocrysts, which indicate high pressures of crystallisation and pyroxene-rich mantle sources (Heinonen et al., 2013). Picritic samples Z1813.1, Z1817.2, and Z1816.3, with fresh euhedral olivine and euhedral/subhedral spinel inclusions (Fig. 2b), were selected for analysis. All of the selected Group

3 samples show evidence of a variable degree of olivine and orthopyroxene accumulation (Heinonen et al., 2013).

3. Analytical methods

For the analysis, the samples were crushed, and the freshest olivine grains were hand-picked, mounted, and polished. Spinel inclusions within olivine hosts which met a minimum size of ~ 8 μm and lacked fractures and alteration textures were selected for analysis, aided by back-scattered electron images. The olivine spinel pairs of the Vestfjella depleted ferropicrite suite (sample AL/B1b-03) and Group 3 dykes (samples Z1813.1, Z1817.2, and Z1816.3) were analysed for Si, Ti, Al, Cr, Fe, Mn, Mg, Ca, and Ni (+P only for olivine) with Cameca SX-100 microprobe at the Department of Earth Sciences, University of Cambridge in two separate analysing periods. Matrix corrections were performed with the Cameca Peak Sight software using the PAP correction method. The microprobe was calibrated using natural and synthetic standards. The acceleration voltage, sample current, and beam diameter for the analyses were 15 kV, 20 or 40 nA (20 for olivine, 40 for spinel), and 1 μm, respectively. The element-specific peak and background count times, standard deviations, and limits of detection are presented in Supplementary Table S1. Special care was taken for setting the analysing conditions for Al: it is a crucial element for the thermometer, but its concentration in olivine is generally very low (< 600 ppm; Coogan et al., 2014). The applied conditions resulted in low limits of detection (≤ 101 ppm) and standard deviations (≤ 20%) for Al in olivine (Supplementary Table S1).

4. Results

The olivine and spinel analyses are presented as major element oxides in Table 1. Olivine compositions represent averages of multiple analyses on the same grain next to the spinel inclusion: the variation in Al content is expressed as σ_{nat}.

The overall compositional characteristics of the phases are similar to previous analytical studies (Heinonen and Luttinen, 2010; Heinonen et al., 2013) with the exception that MnO was not previously measured from the depleted ferropicrite suite spinels (Heinonen and Luttinen, 2010). In addition, our new data does not include the rare $Fo_{89–90}$ olivine phenocrysts identified in Group 3 sample Z1816.3 (Heinonen et al., 2013).

Olivine phenocrysts in the depleted ferropicrite suite sample AL/B1b-03 are very Mg-rich and range from Fo_{88} to Fo_{92}, whereas olivines in Group 3 sample are more Fe-rich and range from Fo_{79} to Fo_{82}, reflecting the higher Fe/Mg of the parental magmas of the latter. The Al_2O_3 contents in olivine range from 0.055 to 0.096 wt. % (Al = 290–510 ppm) in AL/B1b-03 and from 0.026 to 0.035 wt. % (Al = 140–186 ppm) in Group 3 samples (Fig. 3); all analyses are 3σ–8σ above the limit of detection. Spinels in both sample suites are very Cr-rich and exhibit Cr# [Cr/(Cr+Al)] ranging from 0.67–0.78 (Table 1).

All of the olivines have high CaO, and spinels are encapsulated as inclusions within those olivines and have higher TiO_2 than spinels found in mantle peridotites (Fig. 4). These observations indicate that the olivines and spinels crystallised from the parental magma and are not entrained xenocrysts, which is also in accordance with previous studies on these rocks (Heinonen and Luttinen, 2010; Heinonen et al., 2013).

5. Discussion

5.1. Applicability of the Al-in-olivine thermometer

The Al-in-olivine thermometer is not recommended for olivine-spinel pairs that are significantly outside the calibration ranges of the experiments (Wan et al., 2008; Coogan et al., 2014). Here we address the applicability of the thermometer to our samples in terms of spinel Fe^{3+}, Cr#, Ti, and olivine P.

The experiments of Wan et al. (2008) had a relatively tight range of spinel Fe^{3+} [$Fe^{3+}/(Fe^{3+}+Cr+Al) \leq 0.15$]. The additional experiments of Coogan et al. (2014) were performed at higher fO_2 and the authors calibrated the thermometer for more oxidised spinels (spinel $Fe^{3+}/Fe_T \leq 0.35$). All of the analysed spinels in our study have stoichiometrically calculated $Fe^{3+}/Fe_T < 0.35$ (Table 1) and are within the Fe^{3+} calibration range of the thermometer.

The spinels analysed in this study exhibit high Cr# (0.64–0.78) and some of them exceed the Cr# calibration range of the thermometer ($Cr\#^{spl}$ = 0–0.69; Table 1; Coogan et al., 2014). As our calculated temperatures are similar within magma types regardless of the $Cr\#^{spl}$ (Table 1; Fig. 5b) and the correlation of $Cr\#^{spl}$ and $K_D(Al)^{ol\text{-}spl}$ appears to be linear (Wan et al., 2008), we conclude that spinels with high Cr# also give meaningful results.

Our samples exhibit high Ti^{spl} contents (0.029–0.316 per four oxygens; Table 1) relative to the spinels used in the calibration of the thermometer (atomic $Ti^{spl} < 0.025$; Wan et al., 2008; Coogan et al., 2014). We note that the possible effect of high Ti^{spl} on the thermometer has not been studied and Coogan et al. (2014) also use Ti-rich spinels (atomic Ti^{spl} up to 0.07) from Greenland to constrain crystallisation temperatures. The lack of correlation of Ti^{spl} with the calculated temperatures in our data and global LIP data from Coogan et al. (2014) (Fig. 5c) indicates that, for the range of samples presented in these studies, Ti^{spl} does not seem to have a notable effect on the thermometer.

Incorporation of Al into olivine may also take place as a coupled Al-P substitution (Coogan et al., 2014). For olivines with anomalously high P (> 200 ppm), Al^{ol} contents should be extrapolated to P^{ol} = 0 ppm. Phosphorus is below detection limits (≤ 129 ppm; Supplementary Table S1) in all of our samples so a correction is not required.

5.2. Crystallisation temperatures

For the calculation of the crystallisation temperatures of the olivine-spinel pairs we used the experimentally calibrated equation of Coogan et al. (2014):

$$T[K] = 10^4/[0.575 + 0.884Cr\#^{spl} - 0.897\ln(Al_2O_3{}^{ol}/Al_2O_3{}^{spl})] \quad (1)$$

The thermometer reproduces experimental temperatures to within ±25°C (Coogan et al., 2014), but larger errors may be caused by analytical uncertainties and the natural variation in Al^{ol}. Accordingly, we implemented the uncertainty of Al^{ol} in the equation by performing Monte Carlo simulations (n = 5000) for each olivine-spinel pair. We either used analytical σ or natural σ (whichever was larger; Table 1) as the standard deviation for Al^{ol} in the simulations. In all cases, the error of the Al^{ol} measurements exceeds the intrinsic error of the thermometer (±25 °C) such that the errors are ±30–42°C for the depleted ferropicrite suite and ±34–66 °C for Group 3 (Table 1). The relative difference in the errors can be explained by the relatively lower and more variable Al^{ol} in the case of Group 3 (although Al^{ol} analysis of Group 3 samples was more precise; Supplementary Table S1).

The resulting crystallisation temperatures for the olivine-spinel pairs are listed in Table 1 and are plotted against olivine Fo, $Cr\#^{spl}$, and Ti^{spl} in Fig. 5. The temperatures calculated for the depleted ferropicrite suite using Eq. (1) range from 1367±37 °C to 1481±35 °C and for the Group 3 dykes from 1253±64 °C to 1303±40 °C. We were unable to separate the rare $Fo_{89–90}$ olivines from sample Z1816.3 (Heinonen et al., 2013); the presence of these higher Fo phenocrysts indicates that

Group 3 samples have already fractionated to some extent, so their crystallisation temperatures may be somewhat cooler than the true liquidus temperature.

The within-group crystallisation temperatures are not dependent on $Cr\#^{spl}$ (Fig. 5b) or Ti^{spl} (Fig. 5c), but exhibit an expected general positive correlation with olivine Fo (Fig. 5a). One of the depleted ferropicrite suite olivine-spinel pairs (#4) with high olivine Fo ($Fo_{91.8}$), however, shows significantly lower temperature (1367±37 °C) than other pairs with similar olivine Fo ($Fo_{91.2–92.1}$; 1424±30–1481±35 °C; Table 1). Although olivine and spinel of this pair are not texturally different to other pairs, it is possible that the spinel analysis could represent the Cr-poor rim of the crystal and/or that the olivine is zoned in terms of Al (see also Coogan et al., 2014). We regard that the compositions of analysed olivine and spinel may not be in equilibrium in this case and stress the importance of the analysis of multiple olivine-spinel pairs for the determination of crystallisation temperatures when using the Al-in-olivine thermometer.

The maximum crystallisation temperature estimates for the depleted ferropicrite suite acquired using the Al-in-olivine thermometer from the most Mg-rich olivines (1424–1482 °C; $Fo_{91–92}$) are more than 100 °C lower than previously calculated (>1600 °C; Heinonen and Luttinen, 2010) using the olivine-liquid equilibrium equations of Putirka et al. (2007). Similar differences between the results of these two models in general were observed by Coogan et al. (2014). Interestingly, similar liquidus temperatures as given by the Al-in-olivine thermometer are suggested for an accumulated fractional primary melt calculated for the depleted ferropicrite suite sample AL/B1b-03 (1490–1491 °C at 0–3 GPa) with the recent PRIMELT3 software (Herzberg and Asimow, 2015). PRIMELT3 adds olivine to (or subtracts olivine from) a melt composition until it corresponds to a peridotite partial melt composition. The parental melt and olivine compositions predicted by the PRIMELT3 software are very Mg-rich (MgO = 23 wt. % and Fo_{92}, respectively; $K_D(Fe\text{-}Mg)^{ol\text{-}liq}$ = 0.30–0.32), also similar to the suggestions of earlier studies (Heinonen and Luttinen, 2010; see also Table 1 of this study). The compatibility of this approach (originally by Herzberg and O'Hara, 2002) and the Al-in-olivine thermometer was also observed by Coogan et al. (2014). The implied pyroxene-rich source of the Group 3 dykes (Heinonen et al., 2013) hampers the estimation of the liquidus temperatures of their parental melts with the PRIMELT3 software (Herzberg and Asimow, 2008, 2015).

In comparison with Al-in-olivine temperatures calculated for olivine-spinel pairs from MOR settings and other large igneous provinces (LIPs), the depleted ferropicrite suite exhibits temperatures among the highest calculated (Fig. 6). In addition, the temperatures for both Antarctic magma types are relatively high at any given Fo content (Fig. 5a). This may be related to the fact that their parental melts were very Fe-rich (≥ 13 wt. % of FeO^T; Heinonen and Luttinen, 2010; Heinonen et al., 2013), given that Fe-rich melts may crystallise more Fo-poor olivine at higher temperatures compared to melts that have lower Fe contents (see Putirka, 2005).

5.3. Mantle source temperatures

Mantle source temperature is generally described as pressure-independent mantle potential temperature (T_p) that represents the temperature of mantle material if it adiabatically ascended to the Earth's surface without melting (McKenzie and Bickle, 1988). When melting has occurred, its calculation requires correction for the heat of fusion as well as decompression (Cawthorn, 1975) and relies on several assumptions. For example, any given T_p represents average melting conditions and thus assumes that melts segregated from different depths within the melting region are pooled and recombined in crustal magma chambers, integrating their thermal and chemical properties. All the available tools to estimate T_p assume that the mantle source is composed of peridotite and thus we concentrate on Vestfjella depleted ferropicrite suite (derived from peridotite source; Heinonen and Luttinen, 2010) in this section.

One of the simplest methods for deriving T_p of a peridotite source from an olivine crystallisation temperature is provided by Putirka et al. (2007), who assume a two-step process whereby the temperature is first corrected for the temperature drop through fusion, and is then corrected back to 1 atm along an adiabat. The process is described by:

$$T_p[°C] = T^{ol\text{-}liq} + \Delta T_{fus} - P[\partial T/\partial P] \quad (2)$$

The temperature correction for fusion $\Delta T_{fus} = F(\Delta H_{fus}/C_p)$ can be approximated for a lherzolite source using $C_p = 192.4$ J/mol·K^{-1} and $\Delta H_{fus} = 128.3$kJ/mol, and $- P[\partial T/\partial P]$, the adiabatic gradient, can be approximated to be 13.3 °C/GPa (Putirka et al., 2007). Putirka et al. (2007) also provide two different equations to estimate the degree of melting (F) on the basis of major element composition and pressure (given as GPa):

$$F[\%] = -117.2 - 1.62P + 2.12(SiO_2^{liq}) + 4.2(MgO^{liq}) - 3.93(FeO^{liq}) \quad (3)$$

and

$$F[\%] = -105.1 - 2.34P + 1.789(SiO_2^{liq}) + 3.84(MgO^{liq}) - 2.26(FeO^{liq}) \quad (4)$$

These equations are parameterised from experimental peridotite partial melt data (see Putirka et al., 2007). Inputting the parental melt compositions and melting pressures (5–6 GPa) suggested for the depleted ferropicrite suite by Heinonen and Luttinen (2010) to equations (3) and (4) results in F of 24–34 %. Then, replacing $T^{ol\text{-}liq}$ with the highest $T^{ol\text{-}spl}$ values of this study (1464–1481 °C; Table 1) in Eq. (2) results in T_p of ~1540–1640 °C.

Alternatively, T_p can be calculated with the PRIMELT3 software (Herzberg and Asimow, 2015) which gives similar liquidus temperatures for sample AL/B1b-03 as suggested by the Al-in-olivine thermometer (see section 5.2.). As with the equations of Putirka et al. (2007), PRIMELT3 suggests high-degree melting of a garnet peridotite source (F = 31 %) for the parental melt of the sample AL/B1b-03, and the resulting T_p is ~1630 °C (whole-rock composition of AL/B1b-03 used as an input; Heinonen and Luttinen, 2008).

We emphasise that the above T_p's calculated for the depleted ferropicrite suite rely on several simplified assumptions on the thermodynamic properties and composition of the mantle source and should be treated with caution (see Putirka, 2005; Falloon et al., 2007; Putirka et al., 2007; Coogan et al., 2014; Herzberg and Asimow, 2015). The relatively H_2O-rich (~1–2 wt. %; Heinonen and Luttinen, 2010) nature of the parental melts must to some degree undermine the results of models that are based on melting of dry mantle lherzolite (see Stone et al., 1997). Furthermore, the models of Putirka et al. (2007) and Herzberg and Asimow (2015) are only based on Si-Mg-Fe compositions of the parental melt and the mantle source: the F values (24–34 %, see above) suggested by them are too high for the parental melts of the depleted ferropicrite suite source given the observed degree of incompatible trace and minor element (and H_2O) enrichment (e.g., TiO_2 = 1.3–1.4 wt. % in the parental melts; Heinonen and Luttinen, 2008, 2010). For comparison, Heinonen and Luttinen (2010) followed the approach of Herzberg and O'Hara (2002) and suggested an F of 12 % on the basis of not only Si, Mg. and Fe, but also Ti, Al, Mn, Ca, Na, K, Ni, and Cr composition of the estimated parental melts. Using such an F value (and $T^{ol\text{-}spl}$ 1464–1481 °C as $T^{ol\text{-}liq}$ and P of 5–6 GPa) in Eq. (2) results in T_p's of 1464–1495 °C, which are considerably lower than those (e.g., Hole 2015) yielded by the standard models of Putirka et al. (2007) and Herzberg and Asimow (2008, 2015).

The large differences in all of the aforementioned estimates reflect the uncertainties in defining the composition (including volatile content) and degree of melting of the mantle source of the depleted ferropicrite suite. The considerable lithological and compositional heterogeneity of the

sublithospheric mantle (e.g., Warren et al., 2009) poses substantial challenges for defining T_p, especially for compositionally anomalous magma types. Nevertheless, even though the presented mantle source temperatures should be treated with considerable uncertainty, the apparent difference of the crystallisation temperatures between the depleted ferropicrite suite and MORB (~200 °C; Fig. 6) strongly suggests the derivation of the former from sources that are considerably hotter than those beneath modern MORs in general. This conclusion is in agreement with temperatures obtained from other LIPs, also obtained by Al-in-olivine thermometry (Coogan et al., 2014). As the depleted ferropicrite suite is related to the eruption of Karoo CFBs, these vast volcanic eruptions most likely represent melting at the same elevated T_p, the exact value of which is difficult to constrain using the current methods.

We do not provide an estimate for the mantle source temperatures of the Group 3 dykes, because geochemical evidence indicates their derivation from mixed pyroxenite-peridotite sources (Heinonen et al., 2013, 2014). In such a case, it is inappropriate to use the above methods, which are based on parameterisations of experimental studies of peridotite melting; even eq. (2), which calculates T_p independently of liquid composition, requires an estimate of F, for which an understanding of the chemistry of pyroxenite-derived melts is required. There is no clear consensus on the nature of pyroxenite in the mantle, which is reflected in the wide range of bulk compositions on which experiments are performed. Pyroxenite will generally melt more productively and at lower temperatures than peridotite, producing higher fraction melts with higher FeO at a given pressure (e.g. Kogiso et al., 1998). It is expected that pyroxenite-derived melts should record a lower crystallisation temperature at similar T_p than their peridotite-derived counterparts, due to the intersection of the pyroxenite solidus with a given mantle adiabat at higher pressure resulting in an increased ΔT_{fus}. The simple relationship of eq. (2) would also be complicated by heat flow from the surrounding peridotite (Phipps Morgan, 2001). Quantitative modelling of pyroxenite melting is beyond the scope of this study.

5.4. Implications

Given that there is less uncertainty related to the Al-in-olivine thermometer, because knowledge of the parental melt composition (see, e.g., Putirka, 2005; Herzberg et al., 2007) and $K_D(Fe\text{-}Mg)^{ol\text{-}liq}$ (which may be composition- and pressure-dependent; Herzberg and O'Hara, 2002; Toplis, 2005) is not required (Coogan et al., 2014), we consider the Al-in-olivine thermometer to currently provide the best estimate for the crystallisation temperatures of the most Mg-rich magmas of the Karoo CFB province. We regard that the Al-in-olivine thermometer may be especially useful in tracing the thermal history of magmatic systems which have proven to be troublesome for the more traditional thermometers, e.g., if the involved magmas contained volatiles (e.g., Vestfjella depleted ferropicrite suite) or represent anomalous magma compositions from pyroxene-rich sources (e.g., Group 3).

Elevated T_p is frequently attributed to a mantle plume source (e.g. Putirka, 2005; Herzberg et al., 2007). Alternatively, upper mantle temperatures of up to ~1600°C (~200 °C higher than ambient upper mantle) may be caused by supercontinent insulation and favourable plate boundary assemblies (e.g., Coltice et al., 2007, 2009; Rolf et al., 2012). Such a model is in fact supported by the strong trace element and isotopic affinities of the Vestfjella depleted ferropicrite suite to SWIR MORB sources (Heinonen et al., 2010; Heinonen and Kurz, in press). In addition, the results of this study suggest crystallisation temperatures (and possibly mantle potential temperatures) that are ~100 °C lower than estimated by earlier studies on the basis of olivine-melt equilibria and melting models of dry lherzolite source (≥ 1600 °C; Heinonen and Luttinen, 2010; Hole, 2015). It should be emphasised, however, that although the internal heating model is also compatible with the most of the recent structural and geochronological studies on the Karoo LIP (e.g., Le Gall et al., 2002, 2005; Jourdan et al., 2004, 2005, 2006, 2009; Hastie et al., 2014), influence of a mantle plume or plumes for the generation of Karoo CFBs cannot be ruled out (see Ferraccioli et al., 2005; Curtis et al.,

2008). Importantly, the temperature data presented in this study do not discriminate between the two scenarios.

The Al-in-olivine thermometry results of this study and of Coogan et al. (2014) suggest that at least CFBs of the North Atlantic Volcanic Province, Madagascar, and Karoo originated from mantle that was heated above ambient temperatures, irrespective of the heating mechanism. The origin of these provinces is thus difficult to explain solely by models of lithospheric delamination (Elkins-Tanton and Hager, 2000), melting of fertile mantle components (Anderson, 2007), drainage of slowly-accumulated sublithospheric magma reservoir (Silver et al., 2006), or any model that does not include elevated upper mantle temperatures.

6. Summary

We analysed primitive olivine-spinel pairs from Antarctic dyke rocks (Vestfjella depleted ferropicrite suite and Ahlmannryggen Group 3 dykes) related to the Karoo LIP for Al-in-olivine thermometry, which can address crystallisation temperatures without knowledge on melt composition or mineral-melt equilibria. The Vestfjella depleted ferropicrite suite represents the most magnesian magma type known from the Karoo province and both of the analysed magma types are characterised by primary compositions not influenced by the continental lithosphere. The host olivine Fo contents range from 79 to 92 mol. % and the analyses indicate olivine-spinel crystallisation temperatures from 1391±42 °C to 1481±35 °C for the Vestfjella depleted ferropicrite suite and from 1253±64 °C to 1303±40 °C for the Group 3 dykes. The temperatures calculated for the Vestfjella depleted ferropicrite suite are ~100 °C degrees lower than previously estimated using olivine-melt equilibria. Although exact mantle potential temperatures are difficult to estimate due to uncertainties related to degree of melting and mantle source composition, the crystallisation temperatures are compatible with derivation of the most Mg-rich magma type known from the Karoo LIP from a mantle source that was notably heated above ambient upper mantle temperatures.

Acknowledgements

Comments by Dante Canil and Klaus Mezger (Editor) greatly improved the manuscript, and a comment by an anonymous reviewer encouraged us to emphasise the importance of the results. Iris Buisman is warmly thanked for her competent management of the microprobe at Cambridge. Riina Puttonen is thanked for picking some of the olivines from crushed whole-rocks for the analyses. Laurence Coogan provided support in constraining the errors for the thermometer. Arto Luttinen is thanked for their general support of the work. This work has been funded by the Academy of Finland (for J.S.H., Grant no. 252652) and a Natural Environment Research Council studentship (for E.S.J., [NE/J500070/1]).

References

Anderson, D.L., 2005. Large igneous provinces, delamination, and fertile mantle. Elements 1, 271-275. http://dx.doi.org/10.2113/gselements.1.5.271

Anderson, D.L., 2007. The eclogite engine: chemical geodynamics as a Galileo thermometer, in: Foulger, G.R. and Jurdy, D.M., (Eds.), Plates, Plumes, and Planetary Processes. Geological Society of America, Special Publication 430, Boulder, CO, United States, pp. 47-64. http://dx.doi.org/10.1130/2007.2430(03)

Beattie, P., 1993. Olivine-melt and orthopyroxene-melt equilibria. Contrib. Mineral. Petrol. 115, 103-111. http://dx.doi.org/10.1007/bf00712982

Campbell, I.H., 2005. Large Igneous Provinces and the Mantle Plume Hypothesis. Elements 1, 265-269. http://dx.doi.org/10.2113/gselements.1.5.265

Cawthorn, R.G., 1975. Degrees of melting in mantle diapirs and the origin of ultrabasic liquids. Earth Planet. Sci. Lett. 27, 113-120. http://dx.doi.org/10.1016/0012-821X(75)90169-7

Coltice, N., Phillips, B.R., Bertrand, H., Ricard, Y., Rey, P., 2007. Global warming of the mantle at the origin of flood basalts over supercontinents. Geology 35, 391-394. http://dx.doi.org/10.1130/G23240A.1

Coltice, N., Bertrand, H., Rey, P., Jourdan, F., Phillips, B.R., Ricard, Y., 2009. Global warming of the mantle beneath continents back to the Archaean. Gondwana Research 15, 254-266. http://dx.doi.org/10.1016/j.gr.2008.10.001

Coogan, L.A., Saunders, A.D., Wilson, R.N., 2014. Aluminum-in-olivine thermometry of primitive basalts: Evidence of an anomalously hot mantle source for large igneous provinces. Chem. Geol. 368, 1-10. http://dx.doi.org/10.1016/j.chemgeo.2014.01.004

Cox, K.G., 1988. The Karoo province, in: MacDougall, J.D., (Ed.), Continental Flood Basalts. Kluwer Academic Publishers, Dordrecht, Netherlands, pp. 239-271.

Cox, K.G., 1992. Karoo igneous activity, and the early stages of the break-up of Gondwanaland, in: Storey, B.C., Alabaster, T. and Pankhurst, R.J., (Eds.), Magmatism and the Causes of Continental Break-Up. Geological Society of London, Special Publication 68, London, United Kingdom, pp. 137-148. http://dx.doi.org/10.1144/GSL.SP.1992.068.01.09

Curtis, M.L., Riley, T.R., Owens, W.H., Leat, P.T., Duncan, R.A., 2008. The form, distribution and anisotropy of magnetic susceptibility of Jurassic dykes in H.U. Sverdrupfjella, Dronning Maud Land, Antarctica. Implications for dyke swarm emplacement. J. Struct. Geol. 30, 1429-1447. http://dx.doi.org/10.1016/j.jsg.2008.08.004

Duncan, R.A., Hooper, P.R., Rehacek, J., Marsh, J.S., Duncan, A.R., 1997. The timing and duration of the Karoo igneous event, southern Gondwana. J. Geophys. Res. B 102, 18127-18138. http://dx.doi.org/10.1029/97JB00972

Elkins-Tanton, L.T., Hager, B.H., 2000. Melt intrusion as a trigger for lithospheric foundering and the eruption of the Siberian flood basalts. Geophys. Res. Lett. 27, 3937-3940. http://dx.doi.org/10.1029/2000GL011751

Ellam, R.M., 2006. New constraints on the petrogenesis of the Nuanetsi picrite basalts from Pb and Hf isotope data. Earth Planet. Sci. Lett. 245, 153-161. http://dx.doi.org/10.1016/j.epsl.2006.03.004

Falloon, T.J., Danyushevsky, L.V., Ariskin, A., Green, D.H., Ford, C.E., 2007. The application of olivine geothermometry to infer crystallization temperatures of parental liquids: Implications for the temperature of MORB magmas. Chem. Geol. 241, 207-233. http://dx.doi.org/10.1016/j.chemgeo.2007.01.015

Ferraccioli, F., Jones, P.C., Curtis, M.L., Leat, P.T., 2005. Subglacial imprints of early Gondwana break-up as identified from high resolution aerogeophysical data over western Dronning Maud Land, East Antarctica. Terra Nova 17, 573-579. http://dx.doi.org/10.1111/j.1365-3121.2005.00651.x

Ford, C.E., Russell, D.G., Craven, J.A., Fisk, M.R., 1983. Olivine-Liquid Equilibria: Temperature, Pressure and Composition Dependence of the Crystal/Liquid Cation Partition Coefficients for Mg, Fe^{2+}, Ca and Mn. J. Petrol. 24, 256-266. http://dx.doi.org/10.1093/petrology/24.3.256

Furnes, H., Vad, E., Austrheim, H., Mitchell, J.G., Garmann, L.B., 1987. Geochemistry of basalt lavas from Vestfjella and adjacent areas, Dronning Maud Land, Antarctica. Lithos 20, 337-356. http://dx.doi.org/10.1016/0024-4937(87)90015-6

Groenewald, P.B., Moyes, A.B., Grantham, G.H., Krynauw, J.R., 1995. East Antarctic crustal evolution: geological constraints and modelling in western Dronning Maud Land. Precambrian Res. 75, 231-250. http://dx.doi.org/10.1016/0301-9268(95)80008-6

Harris, C., Marsh, J.S., Duncan, A.R., Erlank, A.J., 1990. The petrogenesis of the Kirwan Basalts of Dronning Maud Land, Antarctica. J. Petrol. 31, 341-369. http://dx.doi.org/10.1093/petrology/31.2.341

Harris, C., Watters, B.R., Groenewald, P.B., 1991. Geochemistry of the Mesozoic regional basic dykes of western Dronning Maud Land, Antarctica. Contrib. Mineral. Petrol. 107, 100-111. http://dx.doi.org/10.1007/bf00311188

Hastie, W.W., Watkeys, M.K., Aubourg, C., 2014. Magma flow in dyke swarms of the Karoo LIP: Implications for the mantle plume hypothesis. Gondwana Res. 25, 736-755. http://dx.doi.org/10.1016/j.gr.2013.08.010

Hawkesworth, C.J., Marsh, J.S., Duncan, A.R., Erlank, A.J., Norry, M.J., 1984. The role of continental lithosphere in the generation of the Karoo volcanic rocks: evidence from combined Nd- and Sr-isotope studies, in: Erlank, A.J., (Ed.), Petrogenesis of the Volcanic Rocks of the Karoo Province. Geological Society of South Africa, Special Publication 13, Johannesburg, South Africa, pp. 341-354.

Heinonen, J.S., Kurz, M.D., in press. Low-^{3}He/^{4}He sublithospheric mantle source for the most magnesian magmas of the Karoo large igneous province. Earth Planet. Sci. Lett.

Heinonen, J.S., Luttinen, A.V., 2008. Jurassic dikes of Vestfjella, western Dronning Maud Land, Antarctica: Geochemical tracing of ferropicrite sources. Lithos 105, 347-364. http://dx.doi.org/10.1016/j.lithos.2008.05.010

Heinonen, J.S., Luttinen, A.V., 2010. Mineral chemical evidence for extremely magnesian subalkaline melts from the Antarctic extension of the Karoo large igneous province. Miner. Petrol. 99, 201-217. http://dx.doi.org/10.1007/s00710-010-0115-9

Heinonen, J.S., Carlson, R.W., Luttinen, A.V., 2010. Isotopic (Sr, Nd, Pb, and Os) composition of highly magnesian dikes of Vestfjella, western Dronning Maud Land, Antarctica: A key to the origins of the Jurassic Karoo large igneous province? Chem. Geol. 277, 227-244. http://dx.doi.org/10.1016/j.chemgeo.2010.08.004

Heinonen, J.S., Luttinen, A.V., Riley, T.R., Michallik, R.M., 2013. Mixed pyroxenite–peridotite sources for mafic and ultramafic dikes from the Antarctic segment of the Karoo continental flood basalt province. Lithos 177, 366-380. http://dx.doi.org/10.1016/j.lithos.2013.05.015

Heinonen, J.S., Carlson, R.W., Riley, T.R., Luttinen, A.V., Horan, M.F., 2014. Subduction-modified oceanic crust mixed with a depleted mantle reservoir in the sources of the Karoo continental flood basalt province. Earth Planet. Sci. Lett. 394, 229-241. http://dx.doi.org/10.1016/j.epsl.2014.03.012

Herzberg, C., 2011. Basalts as temperature probes of Earth's mantle. Geology 39, 1179-1180. http://dx.doi.org/10.1130/focus122011.1

Herzberg, C., Asimow, P.D., 2008. Petrology of some oceanic island basalts: PRIMELT2.XLS software for primary magma calculation. Geochem. Geophys. Geosyst. 9. http://dx.doi.org/10.1029/2008GC002057

Herzberg, C., Asimow, P.D., 2015. PRIMELT3 MEGA.XLSM software for primary magma calculation: Peridotite primary magma MgO contents from the liquidus to the solidus. Geochem. Geophys. Geosyst. 8, 563-578. http://dx.doi.org/10.1002/2014GC005631

Herzberg, C., O'Hara, M.J., 2002. Plume-associated ultramafic magmas of Phanerozoic age. J. Petrol. 43, 1857-1883. http://dx.doi.org/10.1093/petrology/43.10.1857

Herzberg, C., Asimow, P.D., Arndt, N.T., Niu, Y., Lesher, C.M., Fitton, J.G., Cheadle, M.J., Saunders, A.D., 2007. Temperatures in ambient mantle and plumes; constraints from basalts, picrites, and komatiites. Geochem. Geophys. Geosyst. 8, http://dx.doi.org/10.1029/2006GC001390

Hole, M.J., 2015. The generation of continental flood basalts by decompression melting of internally heated mantle. Geology 43, 311-314. http://dx.doi.org/10.1130/g36442.1

Jacobs, J., Fanning, C.M., Henjes-Kunst, F., Olesch, M., Paech, H., 1998. Continuation of the Mozambique Belt into East Antarctica: Grenville-age metamorphism and polyphase Pan-African high-grade events in central Dronning Maud Land. J. Geol. 106, 385-406. http://dx.doi.org/10.1086/516031

Jourdan, F., Féraud, G., Bertrand, H., Kampunzu, A.B., Tshoso, G., Le Gall, B., Tiercelin, J.J., Capiez, P., 2004. The Karoo triple junction questioned: evidence from Jurassic and Proterozoic ^{40}Ar/^{39}Ar ages and geochemistry of the giant Okavango dike swarm (Botswana). Earth Planet. Sci. Lett. 222, 989-1006. http://dx.doi.org/10.1016/j.epsl.2004.03.017

Jourdan, F., Féraud, G., Bertrand, H., Kampunzu, A.B., Tshoso, G., Watkeys, M.K., Le Gall, B., 2005. Karoo large igneous province: Brevity, origin, and relation to mass extinction questioned by new $^{40}Ar/^{39}Ar$ age data. Geology 33, 745-748. http://dx.doi.org/10.1130/G21632.1

Jourdan, F., Féraud, G., Bertrand, H., Watkeys, M.K., Kampunzu, A.B., Le Gall, B., 2006. Basement control on dyke distribution in large igneous provinces: case study of the Karoo triple junction. Earth Planet. Sci. Lett. 241, 307-322. http://dx.doi.org/10.1016/j.epsl.2005.10.003

Jourdan, F., Bertrand, H., Schaerer, U., Blichert-Toft, J., Féraud, G., Kampunzu, A.B., 2007a. Major and trace element and Sr, Nd, Hf, and Pb isotope compositions of the Karoo large igneous province, Botswana-Zimbabwe: lithosphere vs mantle plume contribution. J. Petrol. 48, 1043-1077 http://dx.doi.org/10.1093/petrology/egm010

Jourdan, F., Féraud, G., Bertrand, H., Watkeys, M.K., 2007b. From flood basalts to the inception of oceanization: example from the $^{40}Ar/^{39}Ar$ high-resolution picture of the Karoo large igneous province. Geochem. Geophys. Geosyst. 8, http://dx.doi.org/10.1029/2006GC001392

Jourdan, F., Bertrand, H., Feraud, G., Le Gall, B., Watkeys, M.K., 2009. Lithospheric mantle evolution monitored by overlapping large igneous provinces: case study in southern Africa. Lithos 107, 257-268. http://dx.doi.org/10.1016/j.lithos.2008.10.011

Juckes, L.M., 1972. The geology of north-eastern Heimefrontfjella, Dronning Maud Land. British Antarctic Survey, Scientific Report 65, 44 p.

Kamenetsky, V.S., Crawford, A.J., Meffre, S., 2001. Factors controlling chemistry of magmatic spinel: an empirical study of associated olivine, Cr-spinel and melt inclusions from primitive rocks. J. Petrol. 42, 655-671. http://dx.doi.org/10.1093/petrology/42.4.655

Kogiso T., Hirose K., Takahashi E., 1998. Melting experiments on homogeneous mixtures of peridotite and basalt: application to the genesis of ocean island basalts. Earth Planet. Sci. Lett. 162, 45-61. http://dx.doi.org/10.1016/S0012-821X(98)00156-3

Le Gall, B., Tshoso, G., Jourdan, F., Féraud, G., Bertrand, H., Tiercelin, J.J., Kampunzu, A.B., Modisi, M.P., Dyment, J., Maia, M., 2002. $^{40}Ar/^{39}Ar$ geochronology and structural data from the giant Okavango and related mafic dyke swarms, Karoo igneous province, northern Botswana. Earth Planet. Sci. Lett. 202, 595-606. http://dx.doi.org/10.1016/s0012-821x(02)00763-x

Le Gall, B., Tshoso, G., Dyment, J., Basira Kampunzu, A., Jourdan, F., Féraud, G., Bertrand, H., Aubourg, C., Vétel, W., 2005. The Okavango giant mafic dyke swarm (NE Botswana): its structural significance within the Karoo Large Igneous Province. J. Struct. Geol. 27, 2234-2255. http://dx.doi.org/10.1016/j.jsg.2005.07.004

Lee, C.A., Luffi, P., Plank, T., Dalton, H., Leeman, W.P., 2009. Constraints on the depths and temperatures of basaltic magma generation on Earth and other terrestrial planets using new thermobarometers for mafic magmas. Earth Planet. Sci. Lett. 279, 20-33. http://dx.doi.org/10.1016/j.epsl.2008.12.020

Lindström, S., 2005. Palynology of Permian shale, clay and sandstone clasts from the Basen till in northern Vestfjella, Dronning Maud Land. Antarct. Sci. 17, 87-96. http://dx.doi.org/10.1017/S0954102005002476

Luttinen, A.V., Furnes, H., 2000. Flood basalts of Vestfjella: Jurassic magmatism across an Archaean-Proterozoic lithospheric boundary in Dronning Maud Land, Antarctica. J. Petrol. 41, 1271-1305. http://dx.doi.org/10.1093/petrology/41.8.1271

Luttinen, A.V., Rämö, O.T., Huhma, H., 1998. Neodymium and strontium isotopic and trace element composition of a Mesozoic CFB suite from Dronning Maud Land, Antarctica: Implications for lithosphere and asthenosphere contributions to Karoo magmatism. Geochim. Cosmochim. Acta 62, 2701-2714. http://dx.doi.org/10.1016/S0016-7037(98)00184-7

Luttinen, A.V., Leat, P.T., Furnes, H., 2010. Björnnutane and Sembberget basalt lavas and the geochemical provinciality of Karoo magmatism in western Dronning Maud Land, Antarctica. J. Volcanol. Geotherm. Res. 198, 1-18. http://dx.doi.org/10.1016/j.jvolgeores.2010.07.011

Luttinen, A.V., Heinonen, J.S., Kurhila, M., Jourdan, F., Mänttäri, I., Vuori, S.K., Huhma, H., in press. Depleted mantle-sourced CFB magmatism in the Jurassic Africa-Antarctica rift: petrology and $^{40}Ar/^{39}Ar$ and U/Pb chronology of the Vestfjella dyke swarm, Dronning Maud Land, Antarctica. J. Petrol. 56, 919-952. http://dx.doi.org/10.1093/petrology/egv022

Marschall, H.R., Hawkesworth, C.J., Storey, C.D., Dhuime, B., Leat, P.T., Meyer, H.-P., Tamm-Buckle, S., 2010. The Annandagstoppane Granite, East Antarctica: Evidence for Archaean Intracrustal recycling in the Kaapvaal-Grunehogna Craton from zircon O and Hf isotopes. J. Petrol. 51, 2277-2301. http://dx.doi.org/10.1093/petrology/egq057

McKenzie, D., Bickle, M.J., 1988. The volume and composition of melt generated by extension of the lithosphere. J. Petrol. 29, 625-679. http://dx.doi.org/10.1093/petrology/29.3.625

Moyes, A.B., Krynauw, J.R., Barton, J.M.,Jr, 1995. The age of the Ritscherflya Supergroup and Borgmassivet Intrusions, Dronning Maud Land, Antarctica. Antarct. Sci. 7, 87-97. http://dx.doi.org/10.1017/S0954102095000125

Neumann, E.-R, Svensen, H., Galerne, C.Y., Planke, S., 2011. Multistage evolution of dolerites in the Karoo Large Igneous Province, central South Africa. J. Petrol. 52, 959-984. http://dx.doi.org/10.1093/petrology/egr011

Phipps Morgan, J., 2001. Thermodynamics of pressure release melting of a veined plum pudding mantle. Geochem. Geophys. Geosyst. 2, http://dx.doi.org/10.1029/2000GC000049

Putirka, K.D., 2005. Mantle potential temperatures at Hawaii, Iceland, and the mid-ocean ridge system, as inferred from olivine phenocrysts; evidence for thermally driven mantle plumes. Geochem. Geophys. Geosyst. 6, http://dx.doi.org/10.1029/2005GC000915

Putirka, K.D., Perfit, M., Ryerson, F.J., Jackson, M.G., 2007. Ambient and excess mantle temperatures, olivine thermometry, and active vs. passive upwelling. Chem. Geol. 241, 177-206. http://dx.doi.org/10.1016/j.chemgeo.2007.01.014

Riley, T.R., Leat, P.T., Curtis, M.L., Millar, I.L., Duncan, R.A., Fazel, A., 2005. Early-Middle Jurassic dolerite dykes from Western Dronning Maud Land (Antarctica): Identifying mantle sources in the Karoo Large Igneous Province. J. Petrol. 46, 1489-1524. http://dx.doi.org/10.1093/petrology/egi023

Riley, T.R., Curtis, M.L., Leat, P.T., Millar, I.L., 2009. The geochemistry of Middle Jurassic dykes associated with the Straumsvola-Tvora alkaline plutons, Dronning Maud Land, Antarctica and their association with the Karoo large igneous province. Mineral. Mag. 73, 205-226. http://dx.doi.org/10.1180/minmag.2009.073.2.205

Roeder, P.L., Emslie, R.F., 1970. Olivine-liquid equilibrium. Contrib. Mineral. Petrol. 29, 275-289. http://dx.doi.org/10.1007/bf00371276

Rolf, T., Coltice, N., Tackley, P.J., 2012. Linking continental drift, plate tectonics and the thermal state of the Earth's mantle. Earth Planet. Sci. Lett. 351–352, 134-146. http://dx.doi.org/10.1016/j.epsl.2012.07.011

Silver, P.G., Behn, M.D., Kelley, K.A., Schmitz, M., Savage, B., 2006. Understanding cratonic flood basalts. Earth Planet. Sci. Lett. 245, 190-201. http://dx.doi.org/10.1016/j.epsl.2006.01.050

Simkin, T., Smith, J.V., 1970. Minor-element distribution in olivine. J. Geol. 78, 304-325. http://dx.doi.org/10.1086/627519

Spandler, C., O'Neill, H.St.C., 2010. Diffusion and partition coefficients of minor and trace elements in San Carlos olivine at 1,300°C with some geochemical implications. Contrib. Mineral. Petrol. 159, 791-818. http://dx.doi.org/10.1007/s00410-009-0456-8

Stone, W.E., Deloule, E., Larson, M.S., Lesher, C.M., 1997. Evidence for hydrous high-MgO melts in the Precambrian. Geology 25, 143-146. http://dx.doi.org/10.1130/0091-7613(1997)025<0143:EFHHMM>2.3.CO;2

Sweeney, R.J., Duncan, A.R., Erlank, A.J., 1994. Geochemistry and petrogenesis of central Lebombo basalts of the Karoo igneous province. J. Petrol. 35, 95-125. http://dx.doi.org/10.1093/petrology/35.1.95

Toplis, M.J., 2005. The thermodynamics of iron and magnesium partitioning between olivine and liquid; criteria for assessing and predicting equilibrium in natural and experimental systems. Contrib. Mineral. Petrol. 149, 22-39. http://dx.doi.org/10.1007/s00410-004-0629-4

Wan, Z., Coogan, L.A., Canil, D., 2008. Experimental calibration of aluminum partitioning between olivine and spinel as a geothermometer. Am. Mineral. 93, 1142-1147. http://dx.doi.org/10.2138/am.2008.2758

Warren, J.M., Shimizu, N., Sakaguchi, C., Dick, H.J.B., Nakamura, E., 2009. An assessment of upper mantle heterogeneity based on abyssal peridotite isotopic compositions. J. Geophys. Res. B 114. http://dx.doi.org/10.1029/2008JB006186

Wolmarans, L.G., Kent, K.E., 1982. Geological investigations in western Dronning Maud Land, Antarctica - a synthesis. S. Afr. J. Antarc. Res. Suppl. 2, 93 p.

Zhang, X., Luttinen, A.V., Elliot, D.H., Larsson, K., Foland, K.A., 2003. Early stages of Gondwana breakup: the $^{40}Ar/^{39}Ar$ geochronology of Jurassic basaltic rocks from western Dronning Maud Land, Antarctica, and implications for the timing of magmatic and hydrothermal events. J. Geophys. Res. B 108. http://dx.doi.org/10.1029/2001JB001070

Figure captions

Figure 1. Outcrop map of western Dronning Maud Land from Vestfjella to H. U. Svedrupfjella with distribution of Karoo flood basalts and Vestfjella depleted ferropicrite and Ahlmannryggen Group 3 dyke suites. Distribution of Karoo flood basalts and related intrusive rocks in reconstructed Gondwana supercontinent (see Heinonen et al., 2010) is shown in the lower right inset.

Figure 2. Spinel inclusions in olivine phenocrysts in plane-polarised light in samples AL/B1b-03 (a; Vestfjella depleted ferropicrite suite) and Z1816.3 (b; Group 3).

Figure 3. Olivine Fo vs. olivine Al_2O_3 for the Vestfjella depleted ferropicrite suite (VDFP) and Group 3 dykes. Vestfjella olivine-spinel pair that is suspected to be out of equilibrium is shown with a grey symbol (see section 5.2.). LIP and MORB fields are after Coogan et al. (2014). The re-equilibrated olivines of the MORBs from the Siqueiros transform fault are not included (Coogan et al., 2014). Error bars (1σ) either represent the analytical error or natural variation in olivine Al_2O_3, whichever is larger (see Table 1).

Figure 4. Mineral chemistry of the analysed samples from the Vestfjella depleted ferropicrite suite (VDFP) and Group 3 dykes shown in olivine Fo vs. olivine CaO (a) and spinel Al_2O_3 vs. spinel TiO_2 diagrams (b). The dashed line that separates volcanic and plutonic olivines on the basis of CaO in (a) is after Simkin and Smith (1970). Spinel discrimination fields in (b) (LIP = large igneous provinces; OIB = oceanic island basalts; MORB = mid-ocean ridge basalts; ARC = island arcs; Peridotites = mantle peridotites) are after Kamenetsky et al. (2001).

Figure 5. The results of Al-in-olivine thermometry for the Vestfjella depleted ferropicrite suite and Group 3 dykes shown in olivine Fo vs. T (a), spinel Cr# vs. T (b), and spinel Ti vs. T (c) diagrams. Estimated 1σ errors for the temperatures are shown (see. section 5.2). Vestfjella olivine-spinel pair that is suspected to be out of equilibrium is shown with a grey symbol (see. section 5.2). LIP and MORB fields in (a) are after Coogan et al. (2014). Olivine-spinel pairs of the MORBs from the Siqueiros transform fault suffer from re-equilibration of the olivines and are not included (Coogan et al., 2014). LIP olivine-spinel pairs with variable Ti^{spl} analysed by Coogan et al. (2014) shown for reference in (c).

Figure 6. Histogram that shows Al-in-olivine crystallisation temperatures for MORB and LIP olivine-spinel pairs for which olivine Fo contents are ≥ 85 mol. %. Data for MORBs and LIPs other than Karoo (this study) are from Coogan et al. (2014).

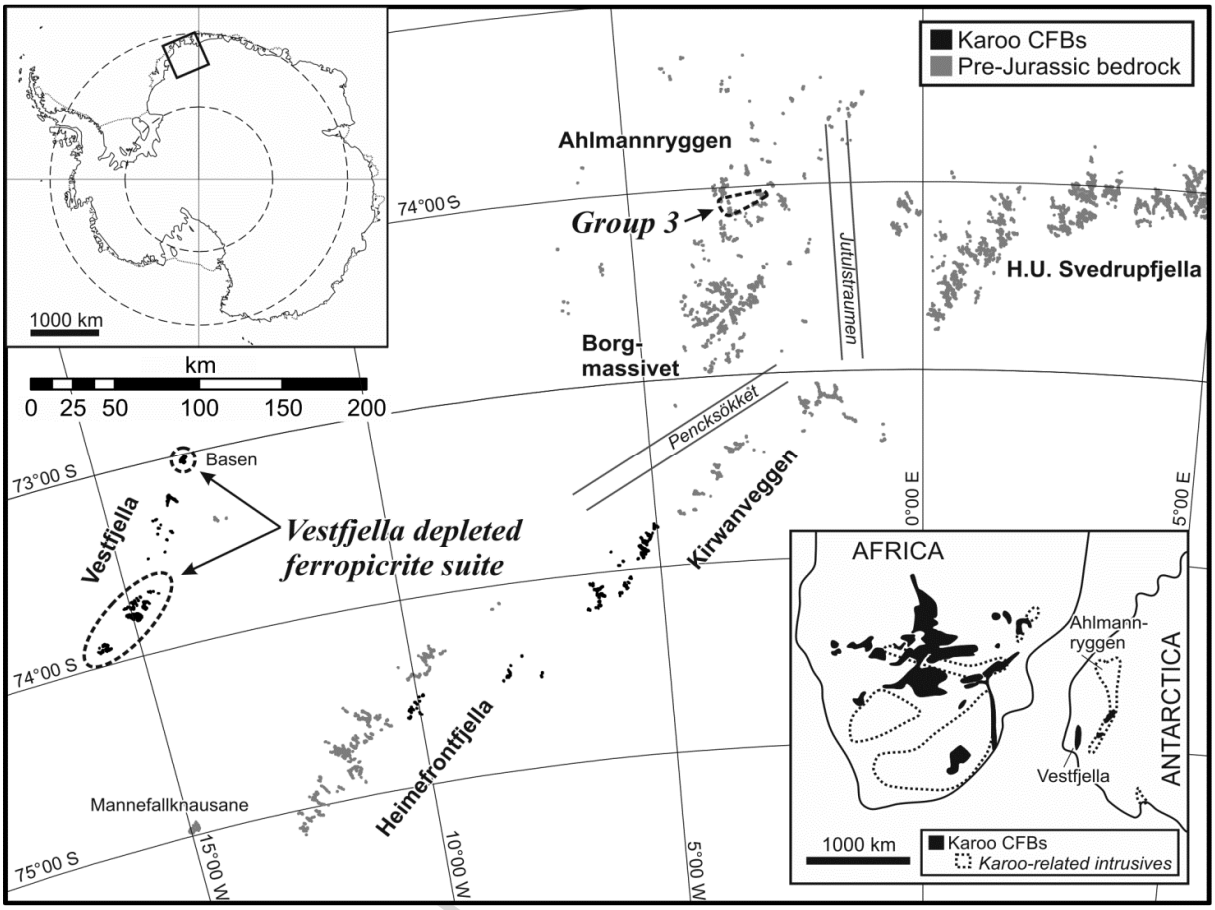

Figure 1

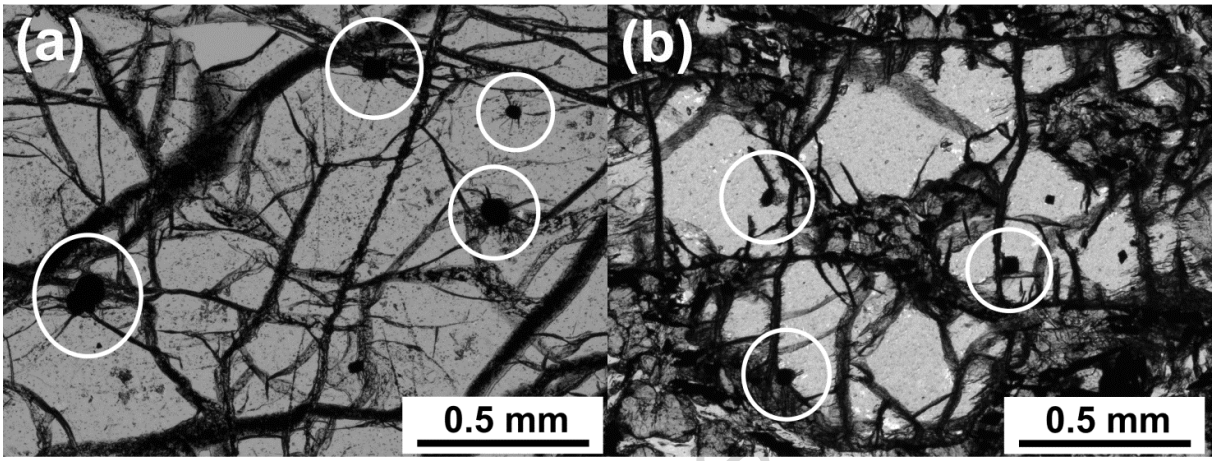

Figure 2

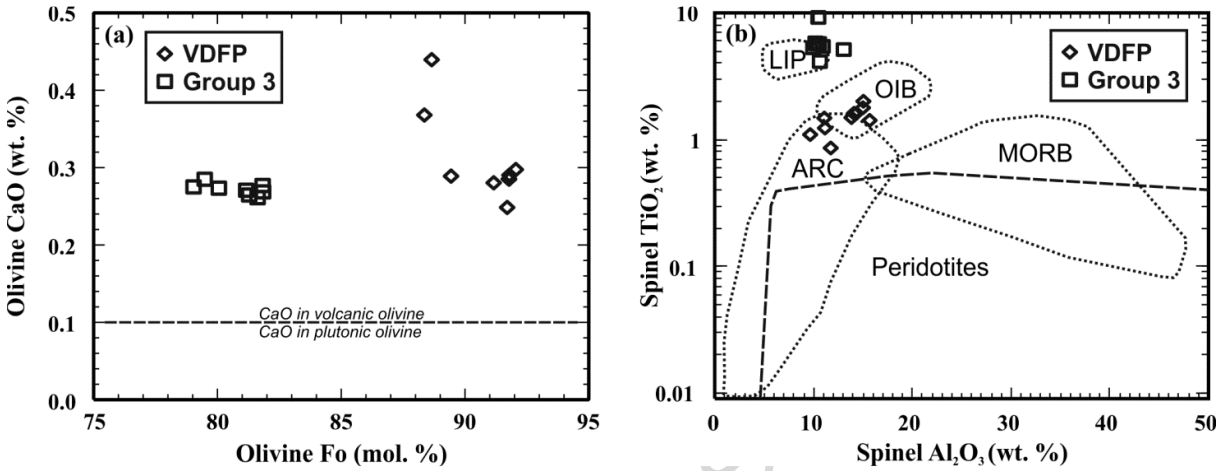

Figure 3

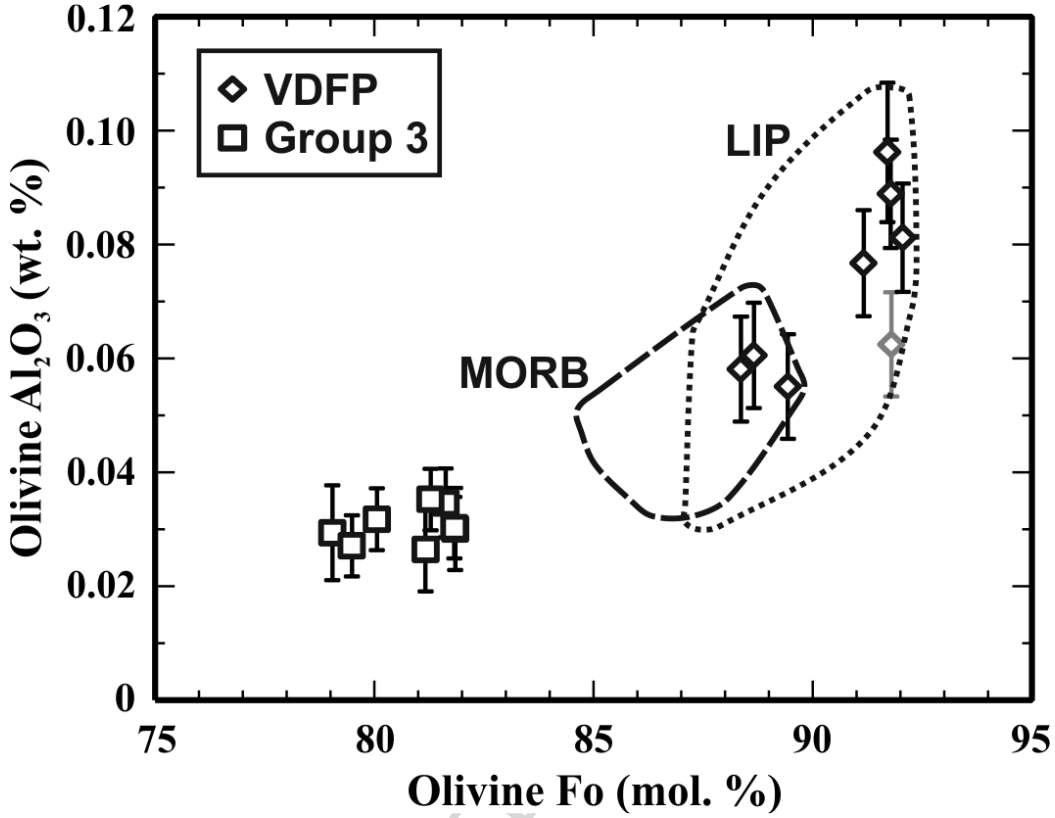

Figure 4

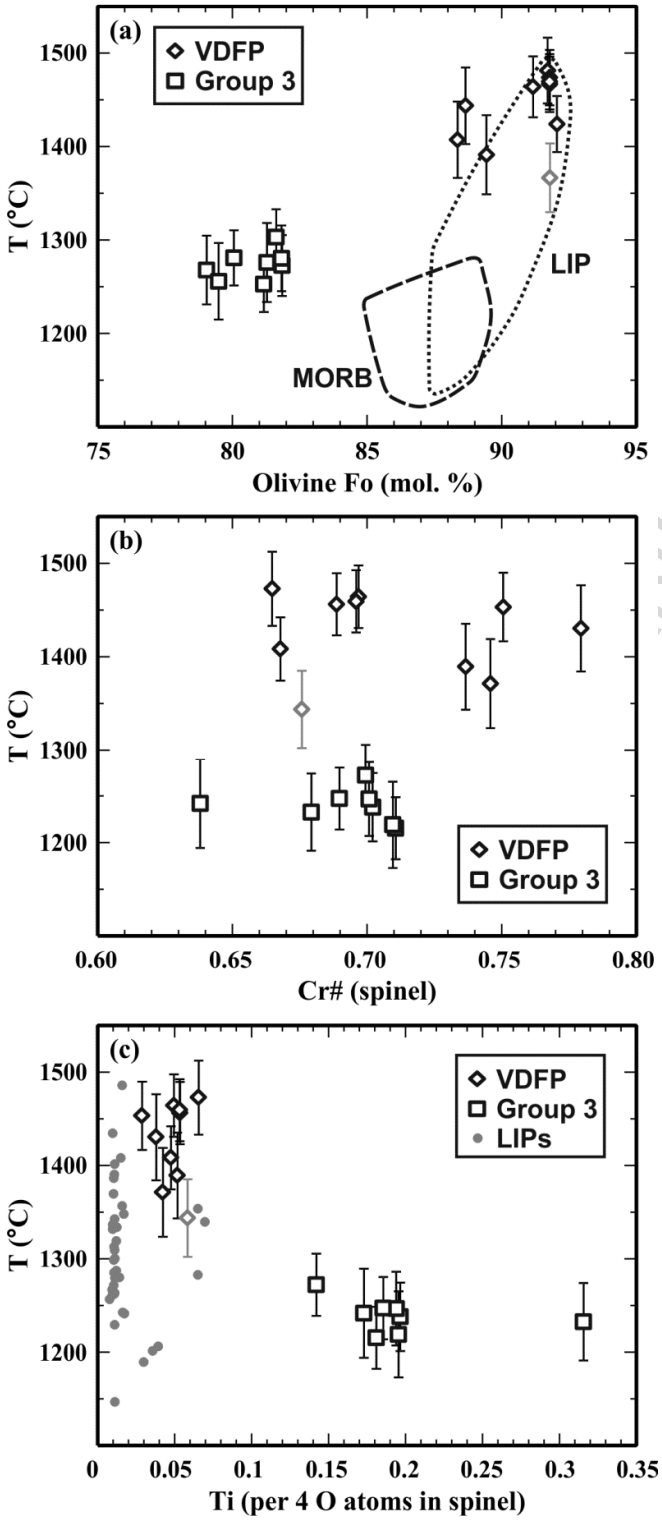

Figure 5

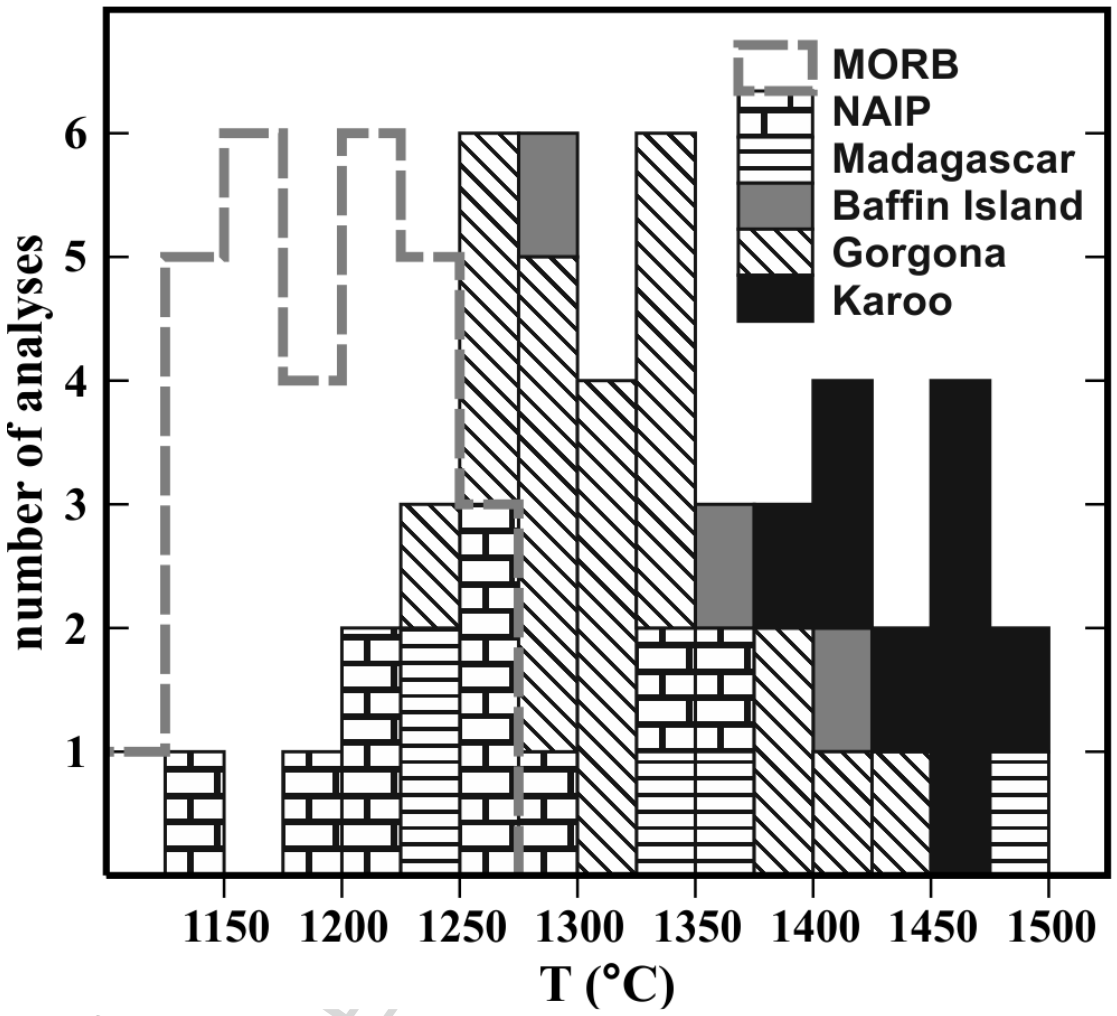

Figure 6

Table 1 Geochemical characteristics and crystallisation temperature estimates for olivine-spinel pairs in sample AL/B1b-03 (B1b; Vestfjella depleted ferropicrite suite) and in samples Z1816.3, Z1813.1, and Z1817.2 (Ahlmannryggen Group 3)

Sample	B1b	B1b	B1b	B1b	B1b	B1b	B1b	B1b	B1b	B1b	B1b	B1b	B1b	B1b	B1b	B1b	B1b	B1b	B1b
ol/spl-pair	1ol	1spl	2ol	2spl	3ol	3splA	3ol	3splB	3ol	3splC	4ol	4spl	5ol	5spl	6ol	6spl	7ol	7spl	8ol	8spl
SiO_2 (wt.%)	40.37	0.16	40.82	0.17	40.70	0.15	40.70	0.16	40.70	0.16	40.73	0.16	39.51	0.09	40.46	0.15	40.43	0.15	40.04	0.12
σ	0.60	0.01	0.60	0.01	0.60	0.01	0.60	0.01	0.60	0.01	0.60	0.01	0.58	0.01	0.60	0.01	0.60	0.01	0.59	0.01
TiO_2 (wt.%)	n.d.	0.88	n.d.	2.04	n.d.	1.64	n.d.	1.52	n.d.	1.65	n.d.	1.81	n.d.	1.12	n.d.	1.26	n.d.	1.45	n.d.	1.51
σ		0.02		0.05		0.04		0.04		0.04		0.04		0.03		0.03		0.03		0.04
Al_2O_3 (wt.%)	0.0767	11.76	0.0962	15.07	0.0889	14.35	0.0889	13.88	0.0889	14.11	0.0625	15.03	0.0605	9.69	0.0551	11.20	0.0812	15.71	0.0581	11.12
σ	0.0093	0.19	0.0098	0.24	0.0095	0.23	0.0095	0.23	0.0095	0.23	0.0092	0.24	0.0093	0.16	0.0092	0.18	0.0095	0.25	0.0092	0.18
σ_{nat}*	0.0089		0.0122		0.0031		0.0031		0.0031		0.0036		0.0071		0.0049		0.0069		0.0057	
LOD*	0.0181		0.0184		0.0181		0.0181		0.0181		0.0183		0.0185		0.0188		0.0183		0.0186	
Cr_2O_3 (wt.%)	0.27	52.78	0.16	44.56	0.17	47.32	0.17	47.56	0.17	48.12	0.10	46.70	0.15	51.02	0.15	48.97	0.16	47.10	n.d.	46.36
σ	0.06	1.28	0.05	1.09	0.05	1.16	0.05	1.16	0.05	1.18	0.05	1.14	0.05	1.24	0.05	1.19	0.05	1.15		1.13
FeO (wt.%)	8.53	20.04	8.03	21.83	7.96	19.94	7.96	20.63	7.96	20.21	7.94	19.55	10.87	25.64	10.12	24.59	7.67	17.93	11.16	26.11
σ	0.39	0.71	0.37	0.77	0.37	0.71	0.37	0.73	0.37	0.72	0.37	0.70	0.47	0.90	0.45	0.86	0.36	0.65	0.48	0.91
MnO (wt.%)	0.16	0.23	0.11	0.24	0.11	0.20	0.11	0.16	0.11	0.21	0.12	0.18	0.20	0.27	0.16	0.23	0.12	0.21	0.16	0.25
σ	0.06	0.04	0.07	0.04	0.06	0.04	0.06	0.04	0.06	0.04	0.06	0.04	0.06	0.04	0.06	0.04	0.06	0.04	0.06	0.04
MgO (wt.%)	49.36	12.39	49.79	13.54	49.85	13.17	49.85	13.06	49.85	13.13	49.84	13.75	47.67	9.80	48.04	10.54	49.85	12.91	47.54	9.74
σ	1.12	0.28	1.13	0.31	1.13	0.30	1.13	0.30	1.13	0.30	1.13	0.31	1.09	0.22	1.09	0.24	1.13	0.29	1.08	0.22
CaO (wt.%)	0.28	0.02	0.25	0.02	0.28	0.04	0.28	0.02	0.28	0.03	0.29	0.04	0.44	0.02	0.29	0.05	0.30	n.d.	0.37	0.02
σ	0.02	0.01	0.02	0.01	0.02	0.01	0.02	0.01	0.02	0.01	0.02	0.01	0.02	0.01	0.02	0.01	0.02		0.02	0.01
NiO (wt.%)	0.43	0.16	0.46	0.29	0.46	0.20	0.46	0.22	0.46	0.25	0.44	0.26	0.41	0.17	0.44	0.19	0.46	0.21	0.44	0.22
σ	0.05	0.04	0.05	0.04	0.05	0.04	0.05	0.04	0.05	0.04	0.05	0.04	0.05	0.04	0.05	0.04	0.05	0.04	0.05	0.04
Total (wt.%)	99.49	98.44	99.74	97.75	99.64	97.01	99.64	97.20	99.64	97.86	99.55	97.49	99.32	97.83	99.73	97.17	99.11	95.68	99.85	95.45
Fo_{ol}	91.2		91.7		91.8		91.8		91.8		91.8		88.7		89.4		92.1		88.4	
Ti_{spl}*		0.029		0.066		0.053		0.050		0.053		0.058		0.038		0.042		0.048		0.052
$Cr\#_{spl}$*		0.751		0.665		0.689		0.697		0.696		0.676		0.779		0.746		0.668		0.737
$(Fe^{3+}/Fe^{T})_{spl}$*		0.24		0.33		0.27		0.29		0.27		0.28		0.27		0.28		0.19		0.29
T (℃)*	1464	1464	1481	1481	1467	1467	1474	1474	1469	1469	1367	1367	1444	1444	1391	1391	1424	1424	1407	1407
σ*	33	33	35	35	30	30	30	30	30	30	37	37	41	41	42	42	30	30	41	41

* σ(nat) = natural variation in olivine Al_2O_3 on the basis of multiple analyses of the same grain; LOD = limit of detection for Al_2O_3 in olivine; Ti_{spl} determined stoichiometrically per four O atoms; Cr# = Cr/(Cr+Al); Fe^{3+}/Fe^{T} calculated stoichiometrically on a four oxygen basis; for calculations of crystallisation temperatures and their σ values, see text

Table 1 continued

Sample	Z1816.3	Z1816.3	Z1813.1	Z1813.1	Z1813.1	Z1813.1	Z1813.1	Z1813.1	Z1817.2	Z1817.2	Z1817.2	Z1817.2	Z1817.2	Z1817.2	Z1817.2	Z1817.2
ol/spl-pair	23ol	23spl	11ol	11spl	39ol	39spl	23ol	23spl	44ol	44spl	40ol	40spl	32ol	32spl	20ol	20spl
SiO_2 (wt.%)	38.96	0.14	39.02	0.08	38.88	0.07	38.71	0.08	38.59	0.07	38.35	0.06	38.89	0.04	39.08	0.10
σ	0.42	0.01	0.42	0.01	0.42	0.01	0.42	0.01	0.42	0.01	0.42	0.01	0.42	0.01	0.42	0.01
TiO_2 (wt.%)	n.d.	5.72	n.d.	5.65	n.d.	5.31	n.d.	4.14	n.d.	5.44	n.d.	9.14	n.d.	5.78	n.d.	5.13
σ		0.12		0.12		0.11		0.09		0.11		0.19		0.12		0.11
Al_2O_3 (wt.%)	0.0301	10.57	0.0303	10.35	0.0265	10.00	0.0346	10.68	0.0318	10.96	0.0294	10.52	0.0271	10.22	0.0352	13.10
σ	0.0054	0.08	0.0054	0.08	0.0054	0.08	0.0054	0.08	0.0054	0.08	0.0054	0.08	0.0054	0.08	0.0054	0.10
σ_{nat}*	0.0072		0.0022		0.0074		0.0060		0.0015		0.0083		0.0014		0.0032	
LOD*	0.0115		0.0117		0.0118		0.0115		0.0117		0.0116		0.0116		0.0115	
Cr_2O_3 (wt.%)	n.d.	37.14	0.09	36.12	n.d.	36.63	0.08	37.05	n.d.	36.32	n.d.	33.22	n.d.	37.23	n.d.	34.41
σ		1.27	0.05	1.24		1.25	0.04	1.27		1.24		1.14		1.27		1.18
FeO (wt.%)	17.06	33.08	17.00	37.37	17.61	37.54	17.24	36.23	18.48	35.61	19.43	39.26	19.03	35.34	17.41	34.76
σ	0.66	1.15	0.65	1.29	0.67	1.30	0.66	1.25	0.70	1.23	0.73	1.36	0.72	1.22	0.67	1.21
MnO (wt.%)	0.21	0.20	0.21	0.30	0.22	0.25	0.20	0.27	0.22	0.26	0.20	0.31	0.22	0.24	0.17	0.24
σ	0.07	0.06	0.07	0.06	0.07	0.06	0.07	0.06	0.07	0.06	0.07	0.06	0.07	0.06	0.07	0.06
MgO (wt.%)	43.13	8.82	42.92	7.23	42.57	7.75	42.96	7.94	41.60	8.17	41.10	5.44	41.36	8.75	42.41	8.76
σ	0.29	0.08	0.29	0.07	0.29	0.08	0.29	0.08	0.29	0.08	0.28	0.06	0.28	0.08	0.29	0.08
CaO (wt.%)	0.27	0.06	0.28	0.03	0.27	0.02	0.26	0.02	0.27	n.d.	0.27	0.06	0.28	0.02	0.26	n.d.
σ	0.02	0.01	0.02	0.01	0.02	0.01	0.02	0.01	0.02		0.02	0.01	0.02	0.01	0.02	
NiO (wt.%)	0.43	0.34	0.40	0.35	0.42	0.35	0.43	0.33	0.43	0.34	0.42	0.31	0.44	0.37	0.47	0.37
σ	0.06	0.06	0.06	0.06	0.06	0.06	0.06	0.06	0.06	0.06	0.06	0.06	0.06	0.06	0.06	0.06
Total (wt.%)	100.19	96.07	99.99	97.46	100.13	97.91	99.94	96.74	99.73	97.18	99.89	98.32	100.35	97.99	99.94	96.88
Fo_{ol}	81.8		81.8		81.2		81.6		80.1		79.0		79.5		81.3	
Ti_{spl}*		0.197		0.194		0.181		0.142		0.185		0.316		0.195		0.173
$Cr\#_{spl}$*		0.702		0.701		0.711		0.699		0.690		0.679		0.710		0.638
$(Fe^{3+}/Fe^{T})_{spl}$*		0.28		0.29		0.32		0.34		0.30		0.17		0.31		0.31
T (℃)*	1273	1273	1280	1280	1253	1253	1303	1303	128 1	1281	1268	1268	1256	1256	1276	1276
σ*	55	55	39	39	64	64	40	40	38	38	66	66	44	44	34	34

Highlights

Re-evaluation of the crystallization temperatures of the most Mg-rich magmas of the Karoo LIP

Most primitive magmas crystallized at temperatures of 1400-1500 °C

Sublithospheric sources of the Karoo LIP heated above ambient upper mantle temperatures